Author Manuscript

Author Manuscript

Author Manuscript

Author Manuscript

HHS Public Access

Author manuscript

J Control Release. Author manuscript; available in PMC 2018 December 10.

Published in final edited form as:

J Control Release. 2017 December 10; 267: 232–239. doi:10.1016/j.jconrel.2017.07.028.

Strategies to Enhance the Distribution of Nanotherapeutics in the Brain

Clark Zhang[a,b], **Panagiotis Mastorakos**[a,c], **Miguel Sobral**[b], **Sneha Berry**[d], **Eric Song**[d], **Elizabeth Nance**[a,e], **Charles G. Eberhart**[f], **Justin Hanes**[a,b,c,g], and **Jung Soo Suk**[a,c,*]

[a]Center for Nanomedicine at the Wilmer Eye Institute, Johns Hopkins University School of Medicine, Baltimore, MD 21231

[b]Department of Biomedical Engineering, Johns Hopkins University School of Medicine, Baltimore, MD 21205

[c]Department of Ophthalmology, The Wilmer Eye Institute, Johns Hopkins University School of Medicine, Baltimore, MD 21231

[d]Zanvyl Krieger School of Arts and Sciences, Johns Hopkins University, Baltimore, MD 21218

[e]Department of Anesthesiology and Critical Care Medicine, Johns Hopkins University, Baltimore, MD 21218

[f]Department of Pathology, Johns Hopkins University School of Medicine, Baltimore, MD 21287

[g]Departments of Oncology, and Pharmacology & Molecular Sciences, Johns Hopkins University School of Medicine, Baltimore, MD, USA

Abstract

Convection enhanced delivery (CED) provides a powerful means to bypass the blood-brain barrier and drive widespread distribution of therapeutics in brain parenchyma away from the point of local administration. However, recent studies have detailed that the overall distribution of therapeutic nanoparticles (NP) following CED remains poor, due to tissue inhomogeneity and anatomical barriers present in the brain, which has limited its translational applicability. Using probe NP, we first demonstrate that a significantly improved brain distribution is achieved by infusing small, non-adhesive NP via CED in a hyperosmolar infusate solution. This multimodal delivery strategy minimizes the hindrance of NP diffusion imposed by the brain extracellular matrix and reduces NP confinement within the perivascular spaces. We further recapitulate the distributions achieved by CED of these probe NP using a most widely explored biodegradable polymer-based drug delivery NP. These findings provide a strategy to overcome several key limitations of CED that have been previously observed in clinical trials.

*Correspondence to J.S. Suk (jsuk@jhmi.edu, 410-614-4526).
Current address: P. Mastorakos, Department of Neurosurgery, University of Virginia, Charlottesville, VA 22908
S. Berry, Department of Cellular and Molecular Medicine, Johns Hopkins University of Medicine, Baltimore, MD 21231
E. Song, Department of Biomedical Engineering, Yale University, New Haven, CT 06511
E. Nance, Department of Chemical Engineering, University of Washington, Seattle, WA 98195

Publisher's Disclaimer: This is a PDF file of an unedited manuscript that has been accepted for publication. As a service to our customers we are providing this early version of the manuscript. The manuscript will undergo copyediting, typesetting, and review of the resulting proof before it is published in its final citable form. Please note that during the production process errors may be discovered which could affect the content, and all legal disclaimers that apply to the journal pertain.

Author Manuscript Author Manuscript Author Manuscript Author Manuscript

Keywords

Brain extracellular matrix; perivascular space; nanoparticle; drug delivery; convection enhanced delivery

Introduction

Most brain diseases are characterized by highly disseminated disease areas throughout the brain tissue. Accordingly, achieving widespread distribution in the brain parenchyma is essential when it comes to the design of therapeutic nanoparticles (NP) for treating brain diseases [1, 2]. Convection enhanced delivery (CED) is an effective delivery strategy to circumvent the blood-brain barrier (BBB) and can theoretically provide widespread NP distribution in the brain by harnessing a pressure-driven bulk flow [1, 3, 4]. However, image-based post-treatment evaluations have revealed that delivery of NP using CED does not readily ensure a therapeutically favorable NP distribution [5]. Intracranially administered NP travel through the brain interstitium, which comprises two distinct spaces, including the intercellular space (ICS) and perivascular space (PVS). NP distribution in the ICS is limited by hindrances imposed by the brain extracellular matrix (ECM) that fills the space [6]. Moreover, preferable flow of NP through, and subsequent confinement within, the low-resistance, fluid-filled PVS hampers widespread distribution of NP, thereby limiting their abilities to reach target cells within the brain [5, 7]. These revelations have shed light on previously terminated CED-based clinical trials that failed to meet their primary and secondary outcomes [8, 9] and have spurred the development of the next generation of NP systems optimized for CED [10, 11]. An improved understanding of the mechanisms that contribute to poor NP distribution following CED will enable the development of strategies to overcome the aforementioned barriers and maximize therapeutic NP distribution within the brain parenchyma.

Conventionally designed NP, even when delivered via the continuous bulk flow of CED, are often found near the point of administration only and cannot travel away through the ICS [12-15]. The brain ECM in the ICS consists of a highly dense, nanoporous network of negatively charged macromolecules and hydrophobic fibrous proteins [16], which serves as a highly impermeable barrier that traps locally administered NP via steric obstruction and/or adhesive interactions, including electrostatic and hydrophobic interactions [6, 17]. We have previously demonstrated that NP up to 114 nm in diameters, if shielded with a dense layer of hydrophilic and neutrally charged polyethylene glycol (PEG; ≥ 9 PEG polymer chains per 100 nm^2 particle surface [6]), resist adhesive interactions with the brain ECM and rapidly diffuse within the healthy brain ICS [6, 18]. We have also shown that the ECM mesh spacings could be smaller depending on the type of tumor [19, 20]. More recently, we demonstrated that a marriage of CED and densely PEGylated NP enabled synergistically enhanced distribution of various therapeutic NP formulations following intracranial administration, while non-PEGylated or conventionally PEGylated NP were unable to do so [13-15, 20].

Author Manuscript Author Manuscript Author Manuscript Author Manuscript

The PVS are cerebrospinal fluid (CSF)-filled canals surrounding large brain vessels, and are responsible for the clearance of metabolites to maintain and regulate the homeostatic balance in the brain [21]. When administered into the brain, NP encounter a relatively higher resistance traveling through the ECM-filled ICS than through the PVS [22]; thus, significant quantities of NP have been microscopically confirmed to traffic through PVS following CED [5, 23, 24]. Once flowed into the PVS, NP remain sequestered therein due to the glia limitans, an anatomical barrier that separates the PVS and ICS [25]. Importantly, NP accumulation within the PVS has been universally observed regardless of delivery modes, including administration via intranasal, intracisternal and intrathecal routes [7, 24, 26]. Given that NP confinement within PVS has been suggested responsible for sub-optimal therapeutic efficacy in clinical trials [23, 27], an effective strategy to address this issue is sorely needed.

Here, we propose a delivery strategy that combines the delivery of non-adhesive NP in conjunction with an osmotic modulation of the brain tissue that renders the brain ECM in the ICS less resistant to NP penetration as well as minimizes undesired NP accumulation in PVS. More specifically, we evaluated the effects of composition and osmolality of infusate solutions on the distribution of densely PEGylated NP [6] in ICS and PVS compartments following CED. Based on this mechanistic study, we then extended the delivery strategy to a similarly engineered, therapeutically relevant drug delivery nanocarrier. The results gleaned from this study may provide a highly translatable strategy that improves the clinical relevance of CED.

Results and Discussion

Enhancing nanoparticle distribution in the brain by reducing adhesive interactions

Fluorescently labeled 40 nm carboxylated polystyrene (PS-COOH) NP probes were modified with exceptionally dense surface PEG coatings according to our previously reported protocol [6]. The average hydrodynamic diameters of PS-COOH and the densely PEGylated NP, PS-PEG, were 51 ± 1.0 and 58 ± 0.2 nm, respectively (Figure 1A). While the surface charge of unmodified PS-COOH, as measured by ζ-potential, was highly negative (-43 ± 2 mV), PS-PEG possessed near neutral surface charge (-3.5 ± 0.8 mV) (Figure 1B), suggesting that the particle surface was densely passivated with a dense PEG layer.

We next assessed *in vivo* distribution of PS-COOH and PS-PEG in mouse (CF-1; Figure S1A) and rat (Sprague Dawley; Figure S1B) brain tissues following co-infusion at the particle concentration of 1 mg/ml. In the brains of both species, non-adhesive PS-PEG NP consistently exhibited significantly greater (~6-7 fold) volume of distribution (Vd) compared to unmodified PS-COOH that were found confined near to the infusion sites (Figure S1). We conclude that even the continuous pressure-driven flow provided by CED cannot adequately overcome the multivalent adhesive interactions that occur between conventional NP (i.e. PS-COOH) and the brain ECM components. Thus, a well-coated, non-adhesive NP surface is likely essential to achieving significant distribution of NP away from the point of administration following CED.

Author Manuscript Author Manuscript Author Manuscript Author Manuscript

In an attempt to address the limited NP distribution, several groups have administered high concentrations of small, conventional NP that saturate the available binding domains throughout the ECM, thereby enabling residual NP to distribute away from the point of infusion [28-30]. We thus sought to determine the correlation between the concentration of infused NP and the Vd of NP achieved following CED at those NP concentrations. The Vd of PS-PEG administered at 0.1, 1, and 25 mg/mL were 10.7-fold, 3.6-fold, and 1.3-fold greater than those of PS-COOH at respective concentrations (Figure 1C). Importantly, PS-PEG achieved uniformly high Vd in a concentration-independent manner, whereas a high NP concentration was required for PS-COOH to be benefitted by the pressure-driven flow provided by CED (Figures 1C, D). The ability to achieve widespread therapeutic distribution at low NP concentrations, observed with CED of non-adhesive NP, may circumvent potential toxicity issues around the use of high NP concentrations for therapeutic delivery to the brain.

Enhancing nanoparticle distribution in the brain by osm otic modulation

The steric obstruction imposed by the ECM structure remains a challenging limitation to non-adhesive NP for achieving widespread distribution in the brain [6, 16], particularly when relatively large NP formulations are required. To overcome this hurdle, we employed a previously explored approach of enhancing therapeutic distribution where brain tissues were modulated in a way that enlarges the mesh spacings of brain ECM [31-34]. Nicholson and coworkers have demonstrated that exposure of brain tissues to modestly hyperosmolar solutions (500 mOsmol/kg) increases the volume of ICS [35], which may minimize the tissue's resistance to NP diffusion. Here, we sought to alter the pore sizes of the mouse brain ECM by using infusate solutions of varying composition and osmolality. We selected hyperosmolar saline and mannitol solutions given that they both have been administered in clinical settings for reducing elevated intracranial pressure [36]. Further, mannitol has been extensively investigated as a hyperosmolar infusate solution for CED of therapeutics in preclinical studies [31, 34, 37]. All infusate solutions evaluated in this study were deemed safe following histological analysis of H&E-stained mouse brain tissues by a board-certified neuropathologist (Figure S2).

To determine the changes in ECM pore sizes following exposure of the brain microenvironment to solutions of different osmolality, we probed the pore sizes of rodent brain tissue by using a previously established *ex vivo* technique [6, 38]. Of note, we ensured that the PS-PEG physicochemical characteristics were unaffected in infusate solutions with varying osmolality (Table 1) to accurately assess the effect of osmolality on the ECM pore size. In contrast, hydrodynamic diameters of PS-COOH markedly increased in a hyperosmolar infusate solution most likely due to the salt-induced surface charge neutralization followed by particle aggregation [39, 40]. We pre-incubated brain slices in water (i.e. hypo-osmolar infusate solution), normal (iso-osmolar; 0.9%) saline or hyperosmolar (3%) saline and then quantified the diffusion rates of subsequently injected non-adhesive PS-PEG probes [6], using multiple particle tracking (MPT) [41]. At a timescale of 1 second, brain slices treated with hyperosmolar 3% saline yielded 1.5-fold greater NP mean squared displacements (MSD) compared to brain slices incubated in normal saline ($p < 0.05$;Figure 2A). The MSD represents a square of distance traveled by a probe at a given time interval [41], and thus, the greater the MSD of non-adhesive NP, the

Author Manuscript Author Manuscript Author Manuscript Author Manuscript

larger the mesh pore. Prior studies have demonstrated that administration of hyperosmolar saline in brain tissue results in enlargement of the ECM mesh spacings as water is drawn out of cells into ICS via an osmotic gradient established by the hyperosmolar saline [32, 35]. Thus, the greater MSD observed with PS-PEG administered in 3% saline is likely attributed to the reduced the steric hindrances experienced by these NP traveling within the brain ICS. On the contrary, treatment of brain slices with hypo-osmolar solution (i.e. water) halved the MSD values of PS-PEG ($p < 0.05$;Figure 2A). This reduced PS-PEG diffusivity is most likely due to an increase in steric hindrances resulted from the engorging of cellular structures driven by water intake and subsequent reduction of ICS [32].

To verify that the osmotic modulation of ICS observed *ex vivo* translates *in vivo, w*e administered NP via CED in saline infusate solutions with varying osmolality and determined their effects on the Vd of NP. We discovered that the Vd of non-adhesive PS-PEG was positively correlated with the osmolality of the infusate solution, whereas Vd of PS-COOH were virtually identical regardless of infusate osmolality (Figure 2B, C). This indicates that even when steric hindrances were minimized, adhesive interactions remained a dominating limitation for the distribution of conventional NP. The Vd of PS-PEG administered in iso- and hyperosmolar infusate solutions were 5.8-fold and 6.8-fold greater than those of co-administrated PS-COOH, respectively ($p < 0.05$). In contrast, the Vd of PS-PEG and PS-COOH were comparable when hypo-osmolar water was used as an infusate solution, suggesting that the elevated steric hindrances stemming from a reduction in ECM pore sizes serve as the dominant limitation to NP distribution. These observations underscore the importance of addressing both types of barrier properties of the brain ECM, namely adhesive interactions and steric obstruction, for enhancing NP distribution in the brain interstitium following CED.

It is critical that the physicochemical properties and colloidal stability of non-adhesive NP in a hyperosmolar infusate solution of interest is retained. We found that increasing the osmolality of mannitol infusate solutions (from 10% to 25%) significantly reduced the PS-PEG diffusivity in brain tissues *ex vivo* (Figure S3A) and distribution *in vivo* (Figure S3B). Of note, osmolality is a colligative property independent of solute type, and thus the contrary findings are unlikely due to an osmotic effect unique to mannitol-based hyperosmolar solutions. Rather, this finding is likely attributed to the marked increase in the hydrodynamic diameters of PS-PEG in 25% mannitol infusate solution (Table S1), more than offsetting the effect of osmotically-driven ECM pore enlargement.

Minimizing nanoparticle flow into perivascular spaces

PVS, also known as Virchow Robin spaces in the brain, serve as a conduit for rapid flow of CSF into the brain from the subarachnoid space [42] and are responsible for the clearance of small metabolic molecules and waste products [21]. Numerous studies have demonstrated that the distribution of therapeutics at large distances away from the injection site takes place predominantly through the PVS [5, 23]. However, preferential trafficking and subsequent sequestration of intracranially administered NP in PVS [43] significantly reduce the available NP dose for treating target cells. Excessive therapeutic buildup within PVS has

Author Manuscript Author Manuscript Author Manuscript Author Manuscript

also resulted in toxic side effects to neighboring macrophages [28], undesired immune responses [23] and an overall reduction in therapeutic efficacy [5, 23].

We hypothesized that the fraction of NP that distributed in favor through the ICS, as opposed to the PVS, would be increased by reducing the resistance of the brain ECM to NP diffusion. We thus investigated the extent of NP trafficking into the PVS when infused in water, 0.9%, and 3% saline. The PS-PEG administered in hypo-osmolar infusate solution (i.e. water) largely accumulated within the PVS, regardless of the distances away from the coronal plane of infusion (Figures 3A-D, Table S2). However, when administered in normal saline, PS-PEG were found in the ICS up to 1.0 mm away from the infusion plane (Figures 3E-H, Table S2), while primarily localized within the PVS at 1.5 mm (Figure 3H, Table S2). Further, PS-PEG infused in hyperosmolar 3% saline were found in both the ICS and PVS up to 1.5 mm away (Figure 3I-L, Table S2), suggesting that NP distribution in ICS may be enhanced by reducing the ECM resistance (i.e. increase in ECM mesh spacings). This simple method of osmotically restoring the balance between NP distribution in ICS and PVS may enhance the translatability of CED in clinics.

It should be noted that, PS-COOH were found solely associated with blood vessels regardless of the infusate osmolality (Figure 3, Table S2). We found that increasing saline concentration reduced the overall distance that PS-COOH trafficked through PVS. Specifically, PS-COOH administered in water and 0.9% saline were found in PVS up to 1.5 mm away from the infusion plane, whereas PS-COOH infused in 3% saline were found in PVS only up to 0.5 mm away. The reduced distance is likely attributed to the poor colloidal stability of PS-COOH in hyperosmolar saline (Table 1); particle aggregation to sizes larger than 1 μm would significantly increase the steric obstruction experienced by NP while traversing through the PVS of arterioles which are sub-1 μm in width [44].

Enabling nanoparticle escape from perivascular spaces

Due to the intrinsically lower physical resistance of the PVS compared to that of ICS [24], NP trafficking in the PVS is inevitable regardless of administration parameters or NP characteristics. Further, NP flowed into the PVS are largely sequestered therein due to an inability to pass through the glia limitans [45], a physical barrier formed by astrocytic foot processes that strictly delineates the PVS from the ICS with only ~20 nm intercellular openings [21, 25, 46]. We hypothesized that by modulating the barrier properties of glia limitans using a hyperosmotic infusate solution, non-adhesive NP would be driven to escape PVS and distribute into the ICS. In particular, we monitored the NP distribution near the lateral striate artery (Figure 4A), a large blood vessel in the brain where a significant NP sequestration was often observed [5], to determine the extent of NP escape from this major artery. When administered in water, both PS-PEG and PS-COOH were confined to PVS (Figure 4B); less than 10% of PS-PEG or PS-COOH fluorescence was detected at a distance of 20 μm from the blood vessel (Figure 4E). Similarly, when administered in 0.9% saline, only 20% of PS-PEG as well as PS-COOH fluorescence was observed at the same distance (Figure 4C, 4F). The limited penetration of PS-PEG through the gila limitans was expected given their significantly larger diameters (~ 60 nm; Figure 1A) compared to the previously determined mesh spacings of this barrier (~ 20 nm; [21]). However, when infused in

Author Manuscript Author Manuscript Author Manuscript Author Manuscript

hyperosmolar 3% saline, while PS-COOH were similarly sequestered within PVS, PS-PEG exhibited markedly improved escape from PVS (Figure 4D, 4G, Video S1). Quantitatively, 65% of PS-PEG fluorescence was observed at a distance of 20 μm with 20% of the fluorescence detectable even at 100 μm. We further analyzed the percent coverage of fluorescent NP outside the PVS but within the brain ICS. Fluorescence of PS-PEG administered in 3% saline was detected across 30% of the ICS found in all captured images, which was significantly greater ($p < 0.05$) than the coverages achieved by other infusate solutions, including 0.9% saline (8% coverage) and water (3% coverage) (Figure 4H).

The migration of non-adhesive NP, but not conventional NP, administered in hyperosmolar solution away from the PVS is likely attributed to the enlargement of mesh spacings of glia limitans, similar to our observation with the brain ECM (Figure 2). Regardless of the infusate solution, conventional NP are unable to reenter the brain ICS due to their adhesive nature that limits their penetration through the glia limitans that is rich in adhesive macromolecules, such as collagen, fibronectin and laminin [47]. To date, only small molecules (e.g. fluorescent dyes, low molecular weight dextrans, etc.) and adeno-associated viruses (20 - 25 nm) have been shown to partition from the PVS into the ICS [7, 21] but here, we demonstrate a strategy that enables the delivery of NP therapeutics as large as 60 nm in diameters out of PVS, through the glia limitans, and into the ICS.

The PVS has been shown to play an important role in progression of numerous neurological diseases. In Alzheimer's disease, dysregulation of the PVS glymphatic system leads to widespread development of amyloid-β plaques [21, 48]. Similarly, PVS, as paths of least resistance, have been implicated in facilitating the migration of malignant gliomas throughout the brain [22, 49], thereby often leading to tumor recurrence. Thus, the strategy to facilitate escape of NP readily traffic to PVS through the glia limitans into the ICS may be exploited to chase the propagation of neurological diseases.

Applying the strategies to biodegradable drug delivery systems

We sought to determine if our findings based on model NP probes (i.e. PS-COOH and PS-PEG) can be translated to therapeutic NP derived from poly(lactic-co-glycolic acid) (PLGA), a FDA-approved polymer most widely used to formulate drug delivery NP [50]. Freshly formulated uncoated PLGA NP and densely PEGylated PLGA (PLGA-PEG) NP exhibited similar hydrodynamic diameters, 80 ± 1 and 71 ± 1 nm, respectively (Table 2). While PLGA-PEG NP retained their colloidal stability (i.e. particle diameter) in 3% saline, uncoated PLGA NP rapidly aggregated up to over 1 μm in the same condition (Table 2), similar to our observation with model uncoated NP (i.e. PS-COOH; Table 1).

Fluorescence-based quantification of NP distribution yielded a statistically significant improvement in the distribution of PLGA-PEG NP as compared to that of PLGA NP, following administration in both 0.9% (Figure 5A) and 3% (Figure 5B) saline via CED ($p < 0.05$). The Vd of PLGA-PEG NP administered in 3% saline was 2.7-fold greater than that of PLGA-PEG NP administered in 0.9% saline (Figure 5C), suggesting that the osmotic modulation resulted in enhanced brain penetration of this non-adhesive drug delivery NP. Further, the hyperosmolar infusate solution facilitated escape of PLGA-PEG NP from PVS (Figures 5D, E), in good agreement with our observation with PS-PEG (Figure 4D). At a

Author Manuscript Author Manuscript Author Manuscript Author Manuscript

distance of 20 μm from the blood vessel, 52% and 12% of PLGA-PEG NP fluorescence was detected when administered in 3% and 0.9% saline, respectively (Figure 5F). In addition, the percent coverage of PLGA-PEG NP within the brain ICS following administration in 3% saline was significantly greater than that of PLGA-PEG NP administered in 0.9% saline (Figure 5G, $p < 0.05$). These results validate our findings with model NP probes that the combined use of non-adhesive surface coatings and hyperosmolar infusate solution synergistically improve distribution of NP in ICS and PVS following CED.

Conclusion

In this study, we developed a simply and safe method to maximize the distribution of therapeutic NP in the brain. Specifically, we introduced a combined approach of administering non-adhesive NP via CED in a hyperosmolar infusate solution that could address major drawbacks currently associated with CED applications, including limited ICS distribution and PVS sequestration of NP. Given the highly ubiquitous nature of many neurological disorders, the strategy may be widely employed to promote widespread delivery of therapeutics throughout the brain.

Materials and Methods

Nanoparticle preparation and characterization

Densely PEGylated NP (i.e. PS-PEG) were engineered by covalently conjugating 5 kDa methoxy-PEG-amine (Creative PEGworks, Winston Salem, NC) onto the surface of dark red fluorescent carboxylated polystyrene beads (PS-COOH; 40 nm in diameters) (Life Technologies, Grand Island, NY), based on our previously published protocol [6]. PLGA-based NP were formulated with PLGA (5kDa; lactide:glycolide ratio of 75:25; Jinan Daigang Biomaterials Co. Ltd., Jinan, China) and PLGA-PEG (25 wt% PEG; Jinan Daigang Biomaterials Co. Ltd.) using the single emulsion method, as we have previously reported [51]. Briefly, PLGA-PEG and PLGA polymers were fluorescently labeled with Alexa Fluor (AF) 647 and AF 555 cadaverine dye (Molecular Probes, Eugene, OR) respectively, as previously described [51]. Polymers were dissolved in dichloromethane and emulsified using a probe sonicator in 0.5 wt% cholic acid (Sigma Aldrich, St. Louis, MO). NP were then subjected to filtration through a 1 μm filter (Whatman, GE Healthcare, Pittsburgh, PA). PLGA-PEG NP were collected and washed using centrifugal filter units (100 kDa MWCO, Millipore, Billerica, MA) at a speed of 3,600 × g for 12 minutes. Likewise, PLGA NP were collected by high speed centrifuge at 22,170 × g for 30 minutes, washed, and resuspended for further use. A small aliquot was lyophilized and weighed to determine the concentration of collected NP. Hydrodynamic diameters and ζ-potentials were measured in 10 mM NaCl solution (pH 7) via dynamic light scattering (DLS) and laser Doppler anemometry techniques, respectively, using a Zetasizer NanoZS (Malvern Instruments, Southborough, MA). For the assessment of colloidal stability, NP were diluted by 200-fold in the following infusate solutions: water, saline (0.9%, 3%) and mannitol (10%, 25%), incubated for 15 minutes at room temperature and hydrodynamic diameters were measured via DLS. For CED experiments, stock PS-PEG and PS-COOH were each diluted by 25-fold in varying infused solutions and mixed at a 1:1 ratio in order to achieve the final NP concentration of 1

Author Manuscript Author Manuscript Author Manuscript Author Manuscript

mg/mL. Additionally, NP at the final concentrations ranging 0.1 - 25 mg/mL in normal (i.e. 0.9%) saline were prepared for evaluating the effect of particle concentration on *in vivo* distribution following CED.

Ex vivo characterization of mesh spacing in mouse brain

The whole brains of female CF-1 mice were harvested and 1.5 mm thick brain slices were prepared, as previously described [6]. Briefly, the harvested brain was rinsed in chilled artificial cerebrospinal fluid and sliced at 1.5 mm intervals using a Zivic mouse brain mold (Zivic Instruments, Pittsburgh, PA). Subsequently, individual brain slices were immersed in varying infusate solutions for 5 minutes. Brain slices were then removed and mounted on a custom-made well and 0.5 μL of fluorescently labeled PS-PEG NP were injected into the cortex. A coverslip was glued on top of the specimen to prevent bulk flow in the tissue, followed by MPT experiment [6]. The particle trajectories were recorded as 20 second movies at a time interval of 66 ms (i.e. 15 frames per second) using an EMCCD camera (Evolve 512; Photometrics, Tuscon, AZ) mounted on an inverted epifluorescence microscope (Axio Observer D1; Zeiss, Thornwood, NY) equipped with a 100× oil-immersion objective (NA 1.3). The MSD values were calculated using a custom-made MATLAB high-throughput NP tracking code.

Convection enhanced delivery

Female CF-1 mice (20 - 30 g) or male Sprague Dawley rats (300 - 400 g) were anesthetized with a mixture of ketamine (75 mg/kg) and xylazine (7.5 mg/kg). For mice, a 2 cm saggital incision was made on the head and a burr hole was made 2 mm lateral to the bregma. All NP solutions or infusate solutions were loaded into a 50 μL Hamilton Neurosyringe with a 33 gauge syringe and set with a 1 mm step (Hamilton, Reno, NV). The syringe was vertically mounted on a Chemyx Nanojet Injector Module (Chemyx, Stafford, TX) which was held on a small animal stereotactic frame (Stoelting, Wood Dale, Il). The loaded syringe was lowered to a depth of 2.5 mm below the mouse dura and a total of 2 μL of the solution was administered over 10 minutes at a rate of 0.2 μL/min. For rats, a burr hole was made 3 mm lateral to the bregma and a total solution of 20 μL of solution was administered at a depth of 3.5 mm at a rate of 0.33 μL/min. In both species, the cannula was allowed to sit for 5 minutes following the completion of infusion and was then withdrawn at a rate of 1 mm/min. Subsequently, the treated animals were sutured (Covidien, Mundelein, Il) and placed on a heating pad for recovery.

In vivo safety of infusate solutions

Following intracranial administration of the various infusate solutions without NP, CF-1 mice were monitored for adverse signs of toxicity. Mice were sacrificed either 1 hour or 72 hours post-administration. Brain tissues were harvested and fixed in formalin for 24 hours, followed by H&E staining conducted by the Johns Hopkins Reference Histology Laboratory. The point of infusion was identified by the tissue cavity imparted by the needle and the region immediately adjacent was imaged and evaluated for evidence of toxicity or hemorrhage by a board-certified neuropathologist (C.G.E.).

Author Manuscript Author Manuscript Author Manuscript Author Manuscript

Quantification of in vivo nanoparticle distribution

Animals were sacrificed 1 hour post-administration of NP, and the brain tissues were fixed in formalin for 24 hours and subsequently exposed to a 10%, 20%, and 30% sucrose gradient. Subsequently, the brain tissues were mounted and cryosectioned at a thickness of 50 μm (Leica Biosystems, Buffalo Grove, Il). The brain slices covering ± 1.5 mm from the infusion site were carefully obtained, fixed with Dako fluorescence mounting medium (Dako, Carpinteria, CA) and imaged using a Zeiss confocal 710 laser scanning microscope (Zeiss) through the GFP and Cy5 channels at 5× magnification. The presence of background fluorescence was determined by comparing to the striatum of the contralateral hemisphere without NP infusion. The images of brain slices were quantified for the fluorescent distribution of NP using a custom-made MATLAB script [13-15, 52], thresholding the images at 10% of the maximum intensity (Figure S4). Fluorescent distribution of NP in the ventricles or white matter tracts were avoided and not included in the quantification. The area of distribution calculated from each slice was multiplied by the slice thickness of 50 μm and summated across all images to estimate the total Vd. If a slice was lost during cryosection procedure, the area of distribution was taken as the average of the previous and following slices. Rarely was more than one slice lost from each brain specimen. Further, to ensure that the observed Vd differences between the PS-COOH and PS-PEG nanoparticles was not due to the use of different channels (i.e. GFP and Cy5 channels, respectively), we switched the fluorescent markers and confirmed that PS-PEG NP (Yellow-green, GFP) exhibited significantly enhanced distribution as compared to PS-COOH NP (Dark-red, Cy5).

For investigating the effect of NP concentration on the Vd following CED, a different quantification method was employed to ensure that the Vd at the lowest NP concentration was fully captured. Briefly, images of brain slices were stacked using Metamorph (Metamorph, Sunnyvale, CA) and then aligned using the StackReg plugin (ImageJ, NIH, Bethesda, MD). A 3D-rendered Vd was generated using Imaris (Bitplane, South Windsor, CT) software employing a threshold of 10% of the maximum fluorescent intensity.

Staining and imaging of blood vessels

The brain tissues that received NP via CED were harvested, fixed and cryosectioned to obtain slices with a 10 μm thickness at designated intervals from the coronal plane of injection (0, 0.5, 1.0 and 1.5 mm). Tissues were mounted on glass slides and immersed in pepsin solution (Dako) at 37° C for 10 minutes. Slides were washed 3 times with PBS and treated with a blocking buffer composed of 5% normal goat serum (Sigma Aldrich) and 1% bovine serum albumin (Sigma Aldrich) in PBS for 1 hour at room temperature. Tissue slices were incubated with primary rabbit anti-mouse collagen IV antibody (Abcam ab6586, Cambridge, MA) diluted at 1:250 in the blocking buffer for 16 hours at 4° C. Tissues were washed 3 times with PBS and incubated with a AF 488-labeled goat anti-rabbit secondary antibody (Life Technologies, Grand Island, NY) diluted at 1:500 in the blocking buffer for 1 hour at room temperature. Tissues were washed 3 times with PBS, and then incubated with DAPI (Life Technologies, Grand Island, NY) at a 1:1000 dilution in PBS for 15 minutes at room temperature. Slides were washed 3 times with PBS and allowed to dry prior to mounting with Dako fluorescence mounting medium (Dako).

Author Manuscript Author Manuscript Author Manuscript Author Manuscript

Using a Zeiss confocal 710 laser scanning microscope, high resolution images (40× magnification) were taken at the designated intervals away from the main NP bulk and imaged for DAPI, collagen IV and different NP. Images were derived from N = 3 mice specimen with at least N = 3 images per animal. Presence of fluorescent NP in PVS and ICS were qualitatively determined in all images collected. For semi-quantitative analysis, presence of NP in ICS and PVS was categorized into the following groups: presence in 90 -100%, 80 - 89%, 20 – 80% and less than 20% of all images (Table S2).

Distribution of NP around lateral striate artery

The lateral striate arteries in the mouse striatum were microscopically visualized by a DAPI stain showing elongated and flattened endothelial cells in the images of brain slices. Co-staining these endothelial cells with blood vessel basement membrane, Collagen IV, confirmed their lining of the striate artery (Figure S5). Images of fluorescently labeled NP in the striate arteries were capture by Zeiss confocal 710 laser scanning microscope at a high resolution (40× magnification). To determine the extent of NP escape from PVS, images were processed through a custom-made MATLAB script. Lines were drawn parallel along the DAPI-stained endothelial cells that delineated the striate arteries. The intensity of NP fluorescence was averaged along the parallel lines at every 10 μm interval up to 100 μm away from the designated striate arteries. At least N = 3 striate artery vessels were quantified in each condition. The percent NP coverage within the parenchymal ICS on each high resolution image (40× magnification) was calculated by using the custom-made MATLAB quantification script which thresholded the images at 10% of the maximum intensity. Flattened, DAPI-stained endothelial cells that line the striate artery were used to delineate the PVS and the ICS and only detectable fluorescence throughout the ICS was quantified. At least N = 3 striate artery images were quantified for each condition.

Statistical Analysis

Statistical analysis between two groups was conducted using a two-tailed Student's *t*-test assuming unequal variances. If multiple comparisons were involved, one-way analysis of variance (ANOVA), followed by post hoc test, was employed, using SPSS 18.0 software (SPSS Inc., Chicago, IL). Differences were determined to be statistically significant at $p < 0.05$.

Supplementary Material

Refer to Web version on PubMed Central for supplementary material.

Acknowledgments

The funding is provided by the National Institutes of Health (R01CA164789, R01EB020147, R01CA197111, R01CA204968 and P30EY001765) and W.W. Smith Charitable Trust (J.S.S). The content is solely the responsibility of the authors and does not necessarily represent the official views of the National Institutes of Health. We also thank Benjamin Schuster and Gregg Duncan for their help in high-throughput MPT analysis.

Author Manuscript Author Manuscript Author Manuscript Author Manuscript

References

1. Allard E, Passirani C, Benoit JP. Convection-enhanced delivery of nanocarriers for the treatment of brain tumors. Biomaterials. 2009; 30:2302–2318. [PubMed: 19168213]
2. Wolak DJ, Thorne RG. Diffusion of macromolecules in the brain: implications for drug delivery. Mol Pharm. 2013; 10:1492–1504. [PubMed: 23298378]
3. Bobo RH, Laske DW, Akbasak A, Morrison PF, Dedrick RL, Oldfield EH. Convection-enhanced delivery of macromolecules in the brain. Proc Natl Acad Sci U S A. 1994; 91:2076–2080. [PubMed: 8134351]
4. Saito R, Tominaga T. Convection-enhanced delivery: from mechanisms to clinical drug delivery for diseases of the central nervous system. Neurol Med Chir (Tokyo). 2012; 52:531–538. [PubMed: 22976134]
5. Krauze MT, Saito R, Noble C, Bringas J, Forsayeth J, McKnight TR, Park J, Bankiewicz KS. Effects of the perivascular space on convection-enhanced delivery of liposomes in primate putamen. Exp Neurol. 2005; 196:104–111. [PubMed: 16109410]
6. Nance EA, Woodworth GF, Sailor KA, Shih TY, Xu Q, Swaminathan G, Xiang D, Eberhart C, Hanes J. A dense poly(ethylene glycol) coating improves penetration of large polymeric nanoparticles within brain tissue. Sci Ttransl Med. 2012; 4:149ra119.
7. Salegio EA, Streeter H, Dube N, Hadaczek P, Samaranch L, Kells AP, San Sebastian W, Zhai Y, Bringas J, Xu T, Forsayeth J, Bankiewicz KS. Distribution of nanoparticles throughout the cerebral cortex of rodents and non-human primates: Implications for gene and drug therapy. Front Neuroanat. 2014; 8:9. [PubMed: 24672434]
8. Kunwar S, Chang S, Westphal M, Vogelbaum M, Sampson J, Barnett G, Shaffrey M, Ram Z, Piepmeier J, Prados M, Croteau D, Pmoedain C, Leland P, Husain SR, Joshi BH, Puri RK. Phase III randomized trial of CED of IL13-PE38QQR vs Gliadel wafers for recurrent glioblastoma. Neuro Oncol. 2010; 12:871–881. [PubMed: 20511192]
9. Lang AE, Gill S, Patel NK, Lozano A, Nutt JG, Penn R, Brooks DJ, Hotton G, Moro E, Heywood P, Brodsky MA, Burchiel K, Kelly P, Dalvi A, Scott B, Stacy M, Turner D, Wooten VG, Elias WJ, Laws ER, Dhawan V, Stoessl AJ, Matcham J, Coffey RJ, Traub M. Randomized controlled trial of intraputamenal glial cell line-derived neurotrophic factor infusion in Parkinson disease. Ann Neurol. 2006; 59:459–466. [PubMed: 16429411]
10. Zhou J, Patel TR, Sirianni RW, Strohbehn G, Zheng MQ, Duong N, Schafbauer T, Huttner AJ, Huang Y, Carson RE, Zhang Y, Sullivan DJ Jr, Piepmeier JM, Saltzman WM. Highly penetrative, drug-loaded nanocarriers improve treatment of glioblastoma. Mol Pharm. 2013; 110:11751–11756.
11. Yin D, Zhai Y, Gruber HE, Ibanez CE, Robbins JM, Kells AP, Kasahara N, Forsayeth J, Jolly DJ, Bankiewicz KS. Convection-enhanced delivery improves distribution and efficacy of tumor-selective retroviral replicating vectors in a rodent brain tumor model. Cancer Gene Ther. 2013; 20:336–341. [PubMed: 23703472]
12. Voges J, Reszka R, Gossmann A, Dittmar C, Richter R, Garlip G, Kracht L, Coenen HH, Sturm V, Wienhard K, Heiss WD, Jacobs AH. Imaging-guided convection-enhanced delivery and gene therapy of glioblastoma. Ann Neurol. 2003; 54:479–487. [PubMed: 14520660]
13. Mastorakos P, Song E, Zhang C, Berry S, Park HW, Kim YE, Park JS, Lee S, Suk JS, Hanes J. Biodegradable DNA nanoparticles that provide widespread gene delivery in the brain. Small. 2015; 12:678–685. [PubMed: 26680637]
14. Mastorakos P, Zhang C, Berry S, Oh Y, Lee S, Eberhart CG, Woodworth GF, Suk JS, Hanes J. Highly PEGylated DNA nanoparticles provide uniform and widespread gene transfer in the brain. Adv Healthc Mater. 2015; 4:1022–1023.
15. Zhang C, Nance EA, Mastorakos P, Chisholm J, Berry S, Eberhart C, Tyler B, Brem H, Suk JS, Hanes J. Convection enhanced delivery of cisplatin-loaded brain penetrating nanoparticles cures malignant glioma in rats. J Control Release. 2017; doi: 10.1016/j.jconrel.2017.03.007
16. Sykova E, Nicholson C. Diffusion in brain extracellular space. Physiol Rev. 2008; 88:1277–1340. [PubMed: 18923183]

Author Manuscript Author Manuscript Author Manuscript Author Manuscript

17. Saito R, Krauze MT, Noble CO, Tamas M, Drummond DC, Kirpotin DB, Berger MS, Park JW, Bankiewicz KS. Tissue affinity of the infusate affects the distribution volume during convection-enhanced delivery into rodent brains: implications for local drug delivery. J Neurosci Methods. 2006; 154:225–232. [PubMed: 16472868]
18. Suk JS, Xu Q, Kim N, Hanes J, Ensign LM. PEGylation as a strategy for improving nanoparticle-based drug and gene delivery. Adv Drug Deliv Rev. 2016; 99(Pt A):28–51. [PubMed: 26456916]
19. Xu Q, Ensign LM, Boylan NJ, Schon A, Gong X, Yang JC, Lamb NW, Cai S, Yu T, Freire E, Hanes J. Impact of Surface Polyethylene Glycol (PEG) Density on Biodegradable Nanoparticle Transport in Mucus ex Vivo and Distribution in Vivo. ACS nano. 2015; 9:9217–9227. [PubMed: 26301576]
20. Mastorakos P, Zhang C, Song E, Kim YE, Park HW, Berry S, Choi WK, Hanes J, Suk JS. Biodegradable brain-penetrating DNA nanocomplexes and their use to treat malignant brian tumors. J Control Release. 2017 In press.
21. Iliff JJ, Wang M, Liao Y, Plogg BA, Peng W, Gundersen GA, Benveniste H, Vates GE, Deane R, Goldman SA, Nagelhus EA, Nedergaard M. A paravascular pathway facilitates CSF flow through the brain parenchyma and the clearance of interstitial solutes, including amyloid beta. Sci Ttransl Med e. 2012; 4:147ra111.
22. Cuddapah VA, Robel S, Watkins S, Sontheimer H. A neurocentric perspective on glioma invasion. Nat Rev Neurosci. 2014; 15:455–465. [PubMed: 24946761]
23. Barua NU, Bienemann AS, Hesketh S, Wyatt MJ, Castrique E, Love S, Gill SS. Intrastriatal convection-enhanced delivery results in widespread perivascular distribution in a preclinical model. Fluids Barriers CNS. 2012; 9:2. [PubMed: 22264361]
24. Foley CP, Nishimura N, Neeves KB, Schaffer CB, Olbricht WL. Real-time imaging of perivascular transport of nanoparticles during convection-enhanced delivery in the rat cortex. Ann Biomed Eng. 2012; 40:292–303. [PubMed: 22009318]
25. Engelhardt B, Coisne C. Fluids and barriers of the CNS establish immune privilege by confining immune surveillance to a two-walled castle moat surrounding the CNS castle. Fluids Barriers CNS. 2011; 8:4. [PubMed: 21349152]
26. Lochhead JJ, Thorne RG. Intranasal delivery of biologics to the central nervous system. Adv Drug Deliv Rev. 2012; 64:614–628. [PubMed: 22119441]
27. Krauze MT, McKnight TR, Yamashita Y, Bringas J, Noble CO, Saito R, Geletneky K, Forsayeth J, Berger MS, Jackson P, Park JW, Bankiewicz KS. Real-time visualization and characterization of liposomal delivery into the monkey brain by magnetic resonance imaging. Brain Res Brain Res Protoc. 2005; 16:20–26. [PubMed: 16181805]
28. MacKay JA, Deen DF, Szoka FC Jr. Distribution in brain of liposomes after convection enhanced delivery; modulation by particle charge, particle diameter, and presence of steric coating. Brain Res. 2005; 1035:139–153. [PubMed: 15722054]
29. Zhou J, Patel TR, Sirianni RW, Strohbehn G, Zheng MQ, Duong N, Schafbauer T, Huttner AJ, Huang Y, Carson RE, Zhang Y, Sullivan DJ Jr, Piepmeier JM, Saltzman WM. Highly penetrative, drug-loaded nanocarriers improve treatment of glioblastoma. Proc Natl Acad Sci U S A. 2013; 110:11751–11756. [PubMed: 23818631]
30. Kroll RA, Pagel MA, Muldoon LL, Roman-Goldstein S, Neuwelt EA. Increasing volume of distribution to the brain with interstitial infusion: dose, rather than convection, might be the most important factor. Neurosurgery. 1996; 38:746–752. [PubMed: 8692395]
31. Neeves KB, Sawyer AJ, Foley CP, Saltzman WM, Olbricht WL. Dilation and degradation of the brain extracellular matrix enhances penetration of infused polymer nanoparticles. Brain Res. 2007; 1180:121–132. [PubMed: 17920047]
32. Chen KC, Nicholson C. Changes in brain cell shape create residual extracellular space volume and explain tortuosity behavior during osmotic challenge. Proc Natl Acad Sci U S A. 2000; 97:8306–8311. [PubMed: 10890922]
33. Mastakov MY, Baer K, Xu R, Fitzsimons H, During MJ. Combined injection of rAAV with mannitol enhances gene expression in the rat brain. Mol Ther. 2001; 3:225–232. [PubMed: 11237679]

Author Manuscript Author Manuscript Author Manuscript Author Manuscript

34. Mamot C, Nguyen JB, Pourdehnad M, Hadaczek P, Saito R, Bringas JR, Drummond DC, Hong K, Kirpotin DB, McKnight T, Berger MS, Park JW, Bankiewicz KS. Extensive distribution of liposomes in rodent brains and brain tumors following convection-enhanced delivery. J Neurooncol. 2004; 68:1–9. [PubMed: 15174514]
35. Kume-Kick J, Mazel T, Vorisek I, Hrabetova S, Tao L, Nicholson C. Independence of extracellular tortuosity and volume fraction during osmotic challenge in rat neocortex. J Physiol. 2002; 542:515–527. [PubMed: 12122149]
36. Kamel H, Navi BB, Nakagawa K, Hemphill JC 3rd, Ko NU. Hypertonic saline versus mannitol for the treatment of elevated intracranial pressure: a meta-analysis of randomized clinical trials. Crit Care Med. 2011; 39:554–559. [PubMed: 21242790]
37. Carty N, Lee D, Dickey C, Ceballos-Diaz C, Jansen-West K, Golde TE, Gordon MN, Morgan D, Nash K. Convection-enhanced delivery and systemic mannitol increase gene product distribution of AAV vectors 5, 8, and 9 and increase gene product in the adult mouse brain. J Neurosci Methods. 2010; 194:144–153. [PubMed: 20951738]
38. Nance E, Timbie K, Miller GW, Song J, Louttit C, Klibanov AL, Shih TY, Swaminathan G, Tamargo RJ, Woodworth GF, Hanes J, Price RJ. Non-invasive delivery of stealth, brain-penetrating nanoparticles across the blood-brain barrier using MRI-guided focused ultrasound. J Control Release. 2014; 189:123–132. [PubMed: 24979210]
39. nanoComposix. Salt Stability of Nanoparticles. 2017:17.
40. Hacker C, Asadi J, Pliotas C, Ferguson S, Sherry L, Marius P, Tello J, Jackson D, Naismith J, Lucocq JM. Nanoparticle suspensions enclosed in methylcellulose: a new approach for quantifying nanoparticles in transmission electron microscopy. Sci Rep. 2016; 6:25275. [PubMed: 27141843]
41. Schuster BS, Ensign LM, Allan DB, Suk JS, Hanes J. Particle tracking in drug and gene delivery research: State-of-the-art applications and methods. Adv Drug Deliv Rev. 2015; 91:70–91. [PubMed: 25858664]
42. Pardridge WM. Drug transport in brain via the cerebrospinal fluid. Fluids Barriers CNS. 2011; 8:7. [PubMed: 21349155]
43. Carare RO, Bernardes-Silva M, Newman TA, Page AM, Nicoll JA, Perry VH, Weller RO. Solutes, but not cells, drain from the brain parenchyma along basement membranes of capillaries and arteries: significance for cerebral amyloid angiopathy and neuroimmunology. Neuropathol Appl Neurobiol. 2008; 34:131–144. [PubMed: 18208483]
44. Patek P. The perivascular spaces of the mammalian brain. Anat Rec. 1944; 88:1–24.
45. Zhang ET, Inman CB, Weller RO. Interrelationships of the pia mater and the perivascular (Virchow-Robin) spaces in the human cerebrum. J Anat. 1990; 170:111–123. [PubMed: 2254158]
46. Papadopoulos MC, Manley GT, Krishna S, Verkman AS. Aquaporin-4 facilitates reabsorption of excess fluid in vasogenic brain edema. FASEB J. 2004; 18:1291–1293. [PubMed: 15208268]
47. Sievers J, Pehlemann FW, Gude S, Berry M. Meningeal cells organize the superficial glia limitans of the cerebellum and produce components of both the interstitial matrix and the basement membrane. J Neurocytol. 1994; 23:135–149. [PubMed: 8195812]
48. Preston SD, Steart PV, Wilkinson A, Nicoll JA, Weller RO. Capillary and arterial cerebral amyloid angiopathy in Alzheimer's disease: defining the perivascular route for the elimination of amyloid beta from the human brain. Neuropathol Appl Neurobiol. 2003; 29:106–117. [PubMed: 12662319]
49. Baker GJ, Yadav VN, Motsch S, Koschmann C, Calinescu AA, Mineharu Y, Camelo-Piragua SI, Orringer D, Bannykh S, Nichols WS, deCarvalho AC, Mikkelsen T, Castro MG, Lowenstein PR. Mechanisms of glioma formation: iterative perivascular glioma growth and invasion leads to tumor progression, VEGF-independent vascularization, and resistance to antiangiogenic therapy. Neoplasia. 2014; 16:543–561. [PubMed: 25117977]
50. Bala I, Hariharan S, Kumar MN. PLGA nanoparticles in drug delivery: the state of the art. Crit Rev Ther Drug Carrier Syst. 2004; 21:387–422. [PubMed: 15719481]
51. Nance E, Zhang C, Shih TY, Xu Q, Schuster BS, Hanes J. Brain-penetrating nanoparticles improve paclitaxel efficacy in malignant glioma following local administration. ACS nano. 2014; 8:10655–10664. [PubMed: 25259648]
52. Berry S, Mastorakos P, Zhang C, Song E, Patel H, Suk JS, Hanes J. Enhancing intracranial delivery of clinically relevant non-viral gene vectors. RSC Advances. 2015; 48:41665–41674.

Author Manuscript Author Manuscript Author Manuscript Author Manuscript

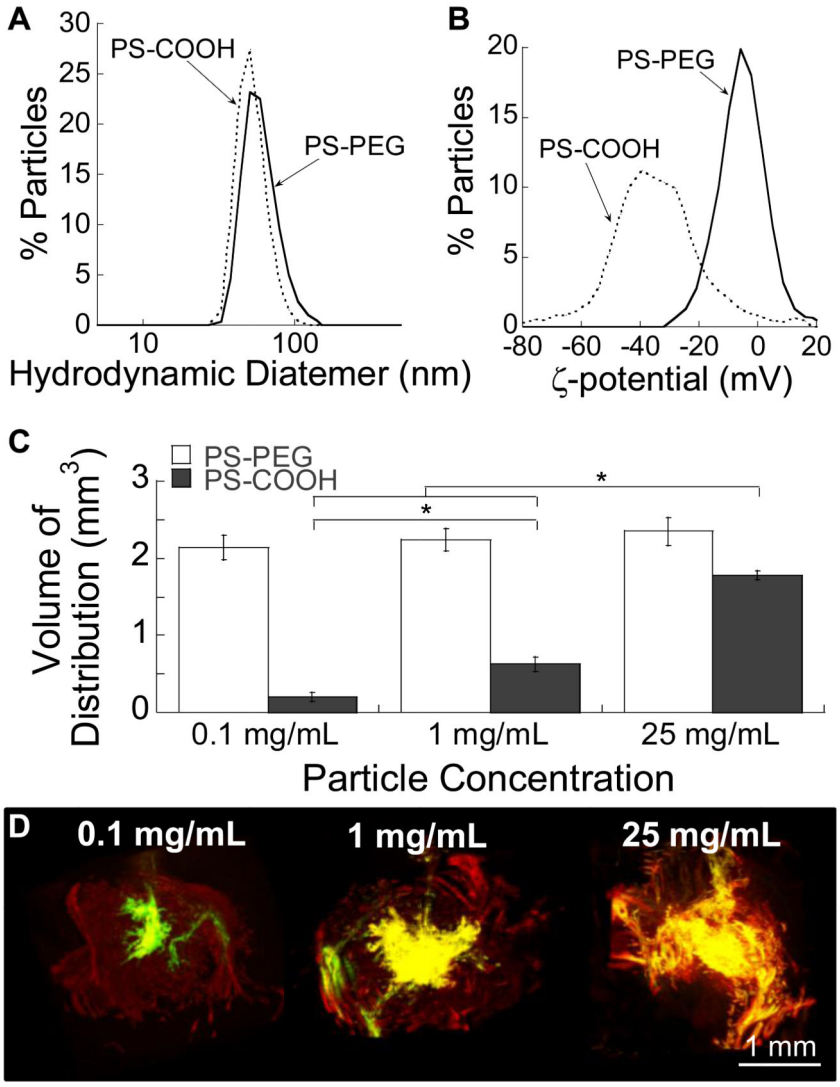

Figure 1. Effect of particle concentration on volume of distribution (Vd) following CED

Physicochemical properties, including **(A)** hydrodynamic diameters and **(B)** ζ-potentials, of model PS NP. **(C)** Quantitative Vd of PS-PEG and PS-COOH NP following CED at varying concentrations. Statistically significant differences are denoted by $*p < 0.05$. **(D)** 3D reconstruction of PS-PEG (red) and PS-COOH (green) NP infused at different concentrations in the mouse striatum following CED. Yellow represents overlay of PS-PEG and PS-COOH.

Author Manuscript Author Manuscript Author Manuscript Author Manuscript

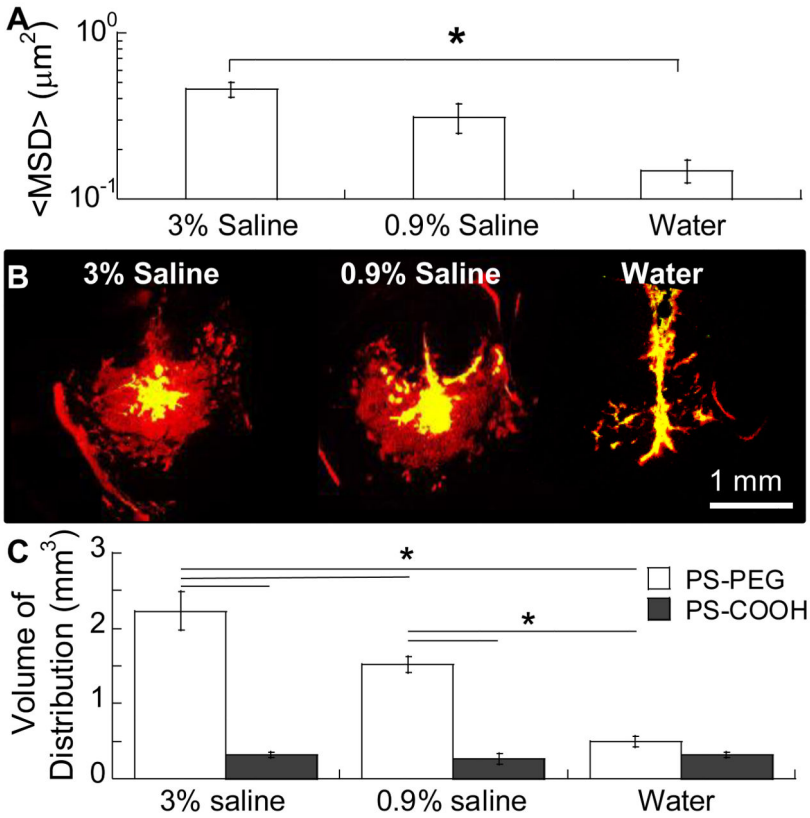

Figure 2. Effect of infusate osmolality on *ex vivo* diffusion and *in vivo* distribution of NP in the mouse brain

(A) Mean squared displacement (<MSD>) of PS-PEG NP in mouse brain slices that were incubated in infusate solutions with varying osmolality. Over 100 NP were tracked per sample (N = 4 mouse brain tissues). *p < 0.05 denotes statistically significant differences. **(B)** Representative slices depicting the coronal plane within the mouse striatum where PS-PEG (red) and PS-COOH (green) NP were infused via CED. Yellow represents overlay of NP. Scale bar = 1 mm. **(C)** Vd of PS-PEG and PS-COOH determined using image-based MATLAB quantification methods. *$p < 0.05$ denotes statistically significant differences.

Author Manuscript Author Manuscript Author Manuscript Author Manuscript

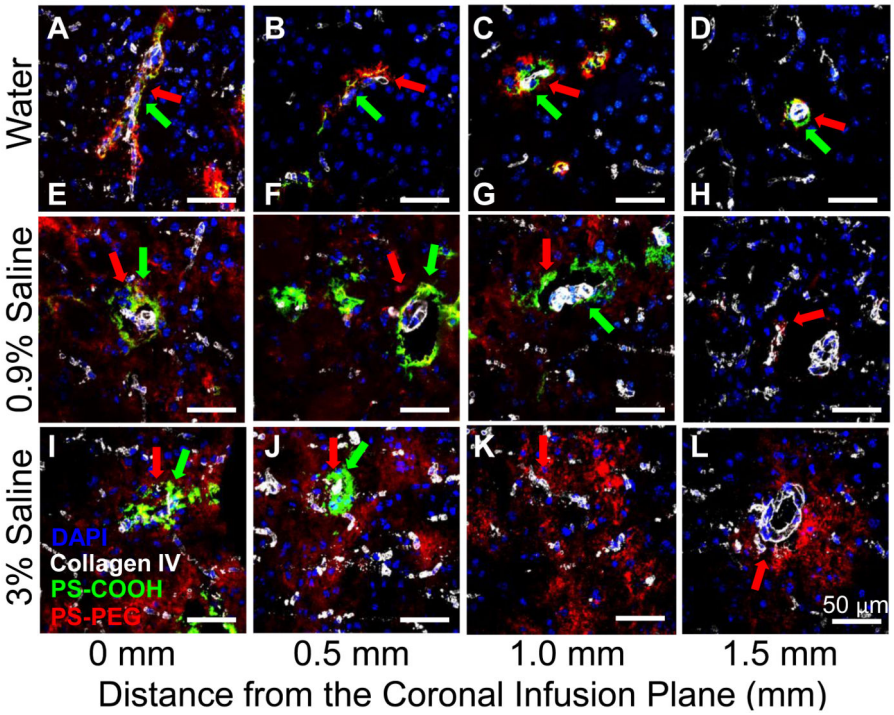

Figure 3. Effect of infusate osmolality on NP distribution in ICS and PVS

Spatial distribution of PS-PEG (red) and PS-COOH (green) NP in ICS and PVS of the mouse brain following CED at varying osmolality of infusate solutions. NP were infused in **(A-D)** water, **(E-H)** 0.9% saline or **(I-L)** 3% saline. White and blue stains represent blood vessels (collagen IV) and cell nuclei (DAPI), respectively. Red and green arrows indicate distribution of PS-PEG and PS-COOH NP, respectively, in PVS. Representative images depict NP distribution in coronal plans of **(A,E,I)** infusion site and **(B,F,J)** 0.5, **(C,G,K)** 1.0 and **(D,H,L)** 1.5 mm away. Scale bar = 50 μm.

Author Manuscript Author Manuscript Author Manuscript Author Manuscript

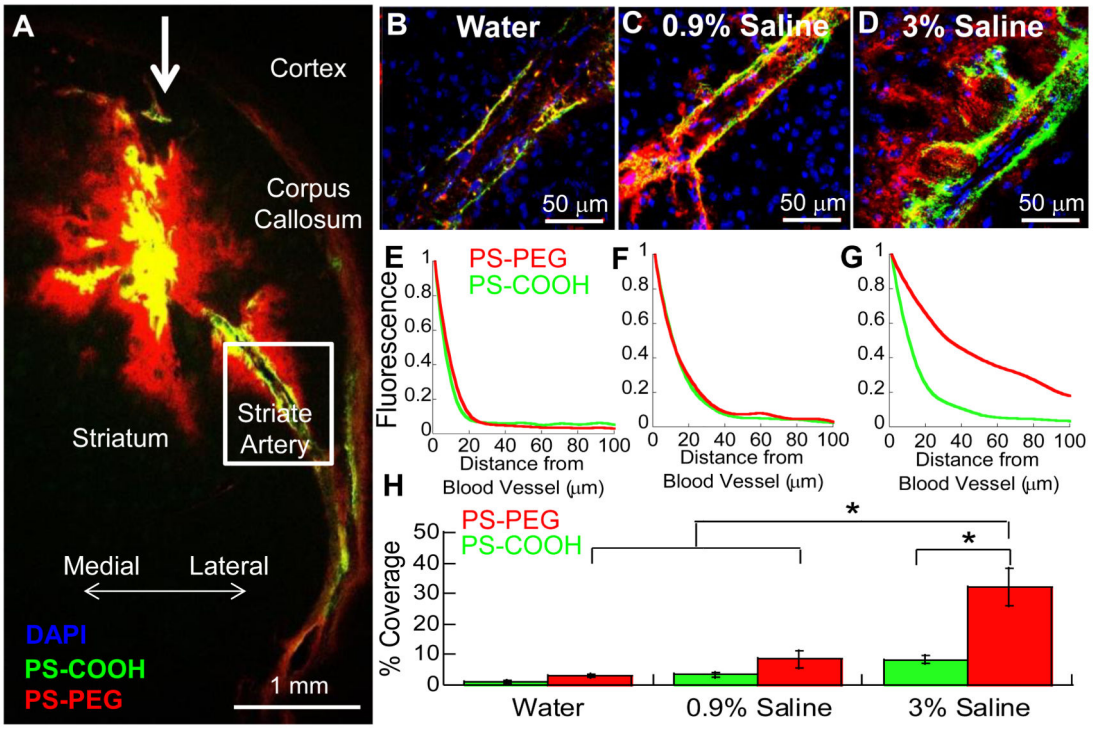

Figure 4. Perivascular distribution of NP following administration via CED in infusate solutions with varying osmolality. (A)

PS-PEG (red) and PS-COOH (green) NP distribution in the striatum 1 hour post-administration vi a CED. White bold-arrow indicates direction of infusion. NP near the striate arteries were imaged following CED in **(B)** water, **(C)** 0.9% saline or **(D)** 3% saline. Blue represents cell nuclei (DAPI). Overlay of NP is represented as yellow. Relative distribution of NP fluorescence in PVS away from the striate artery following CED in **(E)** water, **(F)** 0.9% saline or **(G)** 3% saline. At least N = 3 striate vessels were quantified for each condition. **(H)** Percent coverage of NP fluorescence within the ICS calculated using image-based MATLAB quantification. Statistically significant differences are denoted by *p < 0.05.

Author Manuscript Author Manuscript Author Manuscript Author Manuscript

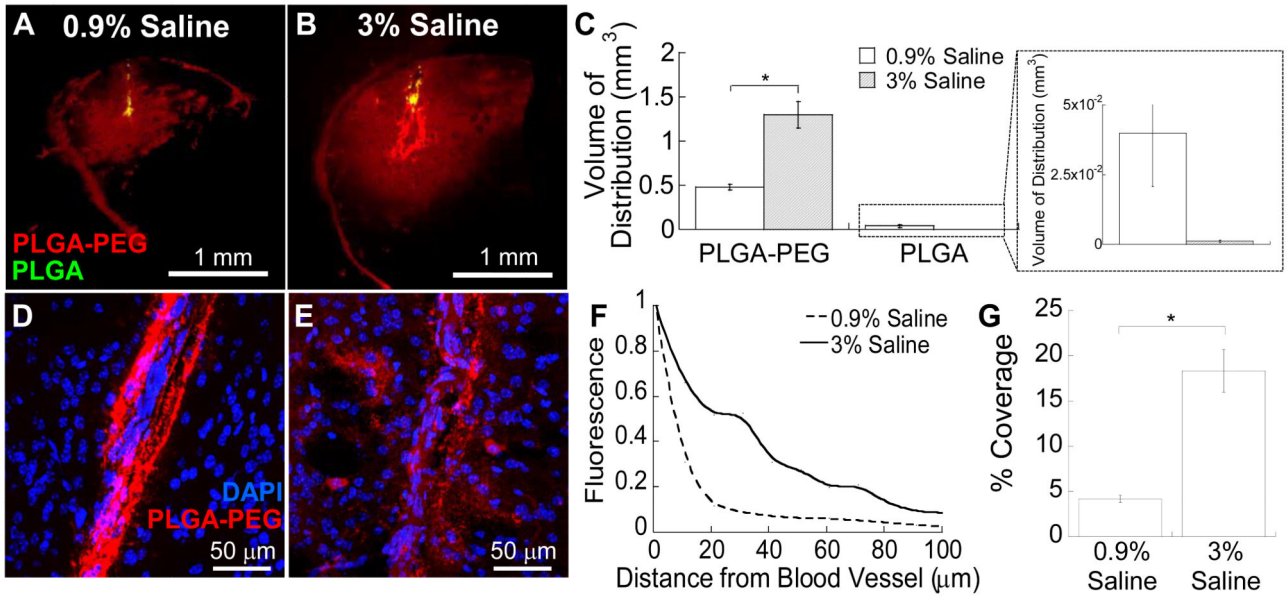

Figure 5. *In vivo* distribution of PLGA-based NP in mouse striatum following administration via CED

Representative coronal images of PLGA-PEG (red) and PLGA (green) NP infused in **(A)** 0.9% saline and **(B)** 3% saline. Data represent the average of N ≥ 3 mouse brain specimen for each condition. **(C)** Quantified Vd of PLGA-PEG and PLGA NP in mouse striatum. Inset depicts the amplified view of PLGA Vd. *p < 0.05 denotes statistical significant difference. High magnification images of PLGA-PEG NP near lateral striate arteries following infusion in **(D)** 0.9% saline and **(E)** 3% saline. Blue indicates cell nuclei (DAPI). **(F)** Relative distribution of NP in PVS away from the striate arteries. **(G)** Percent coverage of PLGA-PEG NP fluorescence within the brain ICS calculated using image-based MATLAB quantification. Statistical significant difference is denoted by *$p < 0.05$.

Author Manuscript

Author Manuscript

Author Manuscript

Author Manuscript

Table 1

Hydrodynamic diameters of PS-PEG and PS-COOH NP in water or saline solutions with varying osmolality.

Infusate Solution		Water	0.9% Saline	3% Saline
Osmolality (mOsm/kg)		0	~300	~1000
Viscosity (cP)		0.89	0.90	0.94
Hydrodynamic Diameter ± SEM (nm)	PS-PEG	58 ± 0.2	61 ± 2	62 ± 0.5
	PS-COOH	51 ± 1	45 ± 2	1330 ± 370

Author Manuscript

Author Manuscript

Author Manuscript

Author Manuscript

Table 2

Hydrodynamic diameters of PLGA-PEG and PLGA NP in saline solutions with varying osmolality.

Particle Type	Hydrodynamic Diameter ± SEM (nm)		
	10 mM NaCl	0.9% Saline	3% Saline
PLGA	80 ± 1	97 ± 13	1377 ± 224
PLGA-PEG	71 ± 1	75 ± 1	75 ± 3